J|A|C|S
ARTICLES
Published on Web 09/24/2004

Crystal Engineering Approach To Forming Cocrystals of Amine Hydrochlorides with Organic Acids. Molecular Complexes of Fluoxetine Hydrochloride with Benzoic, Succinic, and Fumaric Acids

Scott L. Childs,*,† Leonard J. Chyall,‡ Jeanette T. Dunlap,‡ Valeriya N. Smolenskaya,‡ Barbara C. Stahly,‡ and G. Patrick Stahly‡

SSCI, Inc., 3065 Kent Avenue, West Lafayette, Indiana 47906, and Design Science Research, LLC, 1256 Briarcliff Road, Atlanta, Georgia 30306

Received April 1, 2004; E-mail: scott@design-science.info

Abstract: A crystal engineering strategy for designing cocrystals of pharmaceuticals is presented. The strategy increases the probability of discovering useful cocrystals and decreases the number of experiments that are needed by selecting API:guest combinations that have the greatest potential of forming energetically and structurally robust interactions. Our approach involves multicomponent cocrystallization of hydrochloride salts, wherein strong hydrogen bond donors are introduced to interact with chloride ions that are underutilized as hydrogen bond acceptors. The strategy is particularly effective in producing cocrystals of amine hydrochlorides with neutral organic acid guests. As an example of the approach, we report the discovery of three cocrystals containing fluoxetine hydrochloride (**1**), which is the active ingredient in the popular antidepressant Prozac. A 1:1 cocrystal was prepared with **1** and benzoic acid (**2**), while succinic acid and fumaric acid were each cocrystallized with **1** to provide 2:1 cocrystals of fluoxetine hydrochloride:succinic acid (**3**) and fluoxetine hydrochloride:fumaric acid (**4**). The presence of a guest molecule along with fluoxetine hydrochloride in the same crystal structure results in a solid phase with altered physical properties when compared to the known crystalline form of fluoxetine hydrochloride. On the basis of intrinsic dissolution rate experiments, cocrystals **2** and **4** dissolve more slowly than **1**, and **3** dissolves more quickly than **1**. Powder dissolution experiments demonstrated that the solid present at equilibrium corresponds to the cocrystal for **2** and **4**, while **3** completely converted to **1** upon prolonged slurry in water.

Introduction

An important part of the drug development process involves devising a method for delivering the active pharmaceutical ingredient (API). Most APIs are crystalline solids at room temperature and are commonly delivered as a solid oral dosage form such as a tablet. The efficacy of the drug is often dependent on the physical properties of the dosage form, and it is well-established that different solid forms of the same compound have different chemical and physical properties.[1] When improvements in the properties of the API are needed, pharmaceutical scientists often evaluate different solid forms of the API. For an ionizable API, a common approach involves the generation and testing of different salt forms. Salts can effectively provide improved stability, solubility, and crystallinity of the API. Different crystalline polymorphs, hydrates, solvates, and amorphous forms of the API can also provide property improvements, although they are not used as often as salts.

Cocrystallization offers another option that has enormous potential to provide new, stable structures that may improve the properties of an API.[2] A cocrystal is a molecular complex that contains two or more different molecules in the same crystal lattice. Cocrystallization has been underutilized in the pharmaceutical industry, despite the many years API cocrystals have been known.[3−5] However, interest in the subject has grown recently, and a number of new binary cocrystals of APIs have been reported,[6] although in many cases the guest molecules are not pharmaceutically acceptable.

Through a crystal engineering approach, we have developed a method of obtaining multicomponent cocrystals of amine hydrochloride APIs using pharmaceutically acceptable compounds as guests. There is a special and significant opportunity for effective cocrystal formation with amine hydrochlorides that has not been previously recognized. The chloride ion is one of the most preferred anions for salts of cationic APIs. It has been estimated that approximately half of the salts of cationic drugs are marketed as hydrochloride salts.[7] Cocrystallizing the hydrochloride salt of an API presents an opportunity to alter the physical properties of the solid dosage form while simulta-

† Design Science Research, LLC.
‡ SSCI, Inc.

(1) (a) Curatolo, W. *Pharm. Sci. Technol. Today* **1998**, *1*, 387−393. (b) Huang, L. F.; Tong, W. Q. *Adv. Drug Delivery Rev.* **2004**, *56*, 321−334. (c) Bastin, R. J.; Bowker, M. J.; Slater, B. J. *Org. Process Res. Dev.* **2000**, *4*, 427−435. (d) Morris, K. R.; Fakes, M. G.; Thakur, A. B.; Newman, A. W.; Singh, A. K.; Venit, J. J.; Spagnuolo, C. J.; Serajuddin, A. T. M. *Int. J. Pharm.* **1994**, *105*, 209−217.

(2) (a) Datta, S.; Grant, D. J. W. *Nat. Rev. Drug Discov.* **2004**, *3*, 42−57. (b) Rodriguez-Spong, B.; Price, C. P.; Jayasankar, A.; Matzger, A. J.; Rodriguez-Hornedo, N. *Adv. Drug Delivery Rev.* **2004**, *56*, 241−274.

neously retaining the hydrochloride salt of the API in the crystal structure. This methodology is illustrated by the rational synthesis, structural characterization, and dissolution properties of three cocrystals of fluoxetine hydrochloride, which is the API in the popular antidepressant Prozac.

Experimental Section

Fluoxetine hydrochloride (**1**) was obtained from the U.S. Pharmacopeia and used as received. Solvents and reagents were obtained from various commercial suppliers and used as received.

X-ray powder diffraction (XRPD) analyses were carried out on a Shimadzu XRD-6000 diffractometer using Cu Kα radiation. The instrument is equipped with a long fine focus X-ray tube. The tube voltage and amperage were set to 40 kV and 40 mA, respectively. The divergence and scattering slits were set at 1°, and the receiving slit was set at 0.15 mm. Diffracted radiation was detected by a NaI scintillation detector. A $\theta-2\theta$ continuous scan at 3°/min (0.4 s/0.02° step) from 2.5 to 40° 2θ was used. Samples were packed into silicon sample holders. The peak position calibration was verified using a silicon reference standard.

Differential scanning calorimetry (DSC) analyses were carried out on a TA Instruments 2920 differential scanning calorimeter. Each sample was placed into a hermetically sealed aluminum DSC pan containing a pinhole. The sample cell was equilibrated at 25 °C and then heated under a nitrogen purge at a rate of 10 °C/min. Indium metal was used as the calibration standard. Thermogravimetric analyses (TGA) were performed using a TA Instruments Model 2950 thermogravimetric analyzer. Nickel and Alumel were used as the calibration standards. Samples were heated in either aluminum or platinum pans under a stream of nitrogen at rate of 10 °C/min.

Raman spectroscopic analyses were carried out on a Thermo Nicolet 960 spectrometer equipped with an indium gallium arsenide (InGaAs) detector. An excitation wavelength of 1064 nm and approximately 0.4 W of Nd:YVO_4 laser power were used. Each sample was analyzed in a 5 mm diameter glass tube. A total of 256 scans were collected from 3600 to 100 cm^{-1} at a spectral resolution of 4 cm^{-1}. Wavelength calibration was performed using sulfur and cyclohexane.

Moisture sorption/desorption data were collected on a VTI SGA-100 Vapor Sorption Analyzer over a range of 5−95% relative humidity (RH) at 10% RH intervals under a nitrogen purge. Samples were not dried prior to analysis. Equilibrium criteria used for analysis were less than 0.0100% weight change in 5 min. Sodium chloride and poly(vinylpyrrolidone) were used as calibration standards.

Ultraviolet (UV) analyses were carried out on a Beckman-Coulter DU-640 spectrophotometer. The wavelength accuracy of this instrument was verified by calibration with a holmium oxide standard. The photometric accuracy of the instrument was verified by measuring the intensity of the light at the detector when filters of known optical density were placed in the path of the beam. Samples were analyzed in 1 cm cells at 227 nm.

Fluoxetine Hydrochloride Benzoic Acid 1:1 Molecular Complex (2). Fluoxetine hydrochloride (5.00 g, 14.5 mmol) and benzoic acid (1.76 g, 14.4 mmol) were dissolved in 50 mL of acetonitrile with warming. The solution was placed into an open evaporating dish under ambient conditions and allowed to evaporate to a volume of approximately 5 mL. Crystals were isolated by filtration and allowed to dry in the air to give 5.40 g (80% yield) of **2**. Crystals suitable for single-crystal X-ray analysis were obtained by allowing a saturated acetonitrile solution to slowly evaporate.

Fluoxetine Hydrochloride Succinic Acid 2:1 Molecular Complex (3). Fluoxetine hydrochloride (5.00 g, 14.5 mmol) and succinic acid (0.85 g, 7.2 mmol) were dissolved in 55 mL of acetonitrile with warming. The solution was placed into an open evaporating dish under ambient conditions and allowed to evaporate to a volume of approximately 4 mL. Crystals were isolated by filtration and allowed to dry in the air to give 5.40 g (92% yield) of **3**. Crystals suitable for single-crystal X-ray analysis were obtained by seeding a saturated acetonitrile solution and allowing it to evaporate slowly at room temperature.

Fluoxetine Hydrochloride Fumaric Acid 2:1 Molecular Complex (4). Fluoxetine hydrochloride (6.00 g, 17.4 mmol) and fumaric acid (1.01 g, 8.7 mmol) were dissolved in 20 mL of ethanol with warming. The solution was filtered through a 0.2 μm nylon filter, concentrated to a volume of about 8 mL, and cooled in an ice bath for 6 h. The crystals were isolated by filtration and allowed to dry in the air to give 5.74 g (82% yield) of **4**. Crystals suitable for single-crystal X-ray analysis were obtained by allowing a saturated ethanol solution to evaporate slowly at room temperature.

Single-Crystal X-ray Diffraction. Suitable crystals of **2**−**4** were coated with Paratone N oil, suspended in small fiber loops. Crystals of **2** and **3** were placed in a cooled nitrogen gas stream at 100 K on a Bruker D8 APEX CCD sealed-tube diffractometer with graphite-monochromated Mo Kα (0.710 73 Å) radiation, while a crystal of **4** was placed in a cooled nitrogen gas stream at 100 K on a Bruker D8 SMART 1000 CCD sealed-tube diffractometer with graphite-monochromated Cu Kα (1.54178 Å) radiation. Data were measured using a

(3) Examples of API:guest cocrystals are as follows. (a) CSD refcode LABZUJ: Prasad, G. S.; Vijayan, M. *Acta Crystallogr., Sect. B: Struct. Commun.* **1993**, *49*, 348−356. (b) CSD refcode TOPPNP: Aoki, K.; Ichikawa, T.; Koinuma, Y.; Iitaka, Y. *Acta Crystallogr., Sect. B: Struct. Commun.* **1978**, *34*, 2333−2336. (c) CSD refcode ZAYLOA: Zaitu, S.; Miwa, Y.; Taga, T. *Acta Crystallogr., Sect. C: Cryst. Struct. Commun.* **1995**, *51*, 1857−1859. (d) CSD refcode ZEXTIF: Zaitu, S.; Miwa, Y.; Taga, T. *Acta Crystallogr., Sect. C: Cryst. Struct. Commun.* **1995**, *51*, 2390−2392. (e) CSD refcode GEYSAE: Patel, U.; Haridas, M.; Singh, T. P. *Acta Crystallogr., Sect. C: Cryst Struct. Commun.* **1988**, *44*, 1264−1267. (f) CSD refcode VUGMOZ: Caira, M. R. *J. Crystallogr. Spectrosc. Res.* **1992**, *22*, 193−200. (g) CSD refcode PEQBES: Krajewski, K.; Ciunik, Z. *Pol. J. Chem.***1999**, *73*, 1687−1696. (h) CSD refcode SAGQEW: Caira, M. R.; Dekker, T. G.; Liebenberg, W. *J. Chem. Crystallogr.* **1998**, *28*, 11−15. (i) CSD refcode JATMEW: Ishida, T.; In, Y.; Doi, M.; Inoue, M. *Acta Crystallogr., Sect. B: Struct. Commun.* **1989**, *45*, 505−512. (j) CSD refcode SOSBAD: van Roey, P.; Bullion, K. A.; Osawa, Y.; Browne L. J.; Bowman R. M.; Braun D. G. *J. Enzyme Inhib. Med. Chem.* **1991**, *5*, 119−226. (k) CSD refcode LOKRAE: Krajewski, K.; Ciunik, Z. *Pol. J. Chem.* **1999**, *73*, 1687−1696. (l) CSD refcode TAJVOP: van Roey, P.; Bullion, K. A.; Osawa, Y.; Bowman, R. M.; Braun, D. G. *Acta Crystallogr., Sect. C: Cryst. Struct. Commun.* **1991**, *47*, 1015−1018.

(4) Examples of API:API cocrystals are as follows. (a) CSD refcode THOPBA: Nakao, S.; Fujii, S.; Sakaki, T.; Tomita, K. I. *Acta Crystallogr., Sect. B: Struct. Commun.* **1977**, *33*, 1373−1378. (b) CSD refcode VIGVOW: Ghosh, M.; Basak, A. K.; Mazumdar, S. K.; Sheldrick, B. *Acta Crystallogr., Sect, C: Cryst. Struct. Commun.* **1991**, *47*, 577−580. (c) CSD refcode BIGCUP: Shimizu, N.; Nishigaki, S.; Nakai, Y.; Osaki, K. *Acta Crystallogr., Sect. B: Struct. Commun.* **1982**, *38*, 2309−2311. (d) CSD refcode HEKRUK: Giuseppetti, G.; Tadini, C.; Bettinetti, G. P. *Acta Crystallogr., Sect. C: Cryst. Struct. Commun.* **1994**, *50*, 1289−1291. (e) CSD refcode RASSUZ: Bettinetti, G.; Sardone, N. *Acta Crystallogr., Sect. C: Cryst. Struct. Commun.* **1997**, *53*, 594−597. (f) CSD refcode RIWLOY: Sardone, N.; Bettinetti, G.; Sorrenti, M. *Acta Crystallogr., Sect. C: Cryst. Struct. Commun.* **1997**, *53*, 1295−1299. (g) CSD refcode QQQEYV10: Patel, U.; Singh, T. P. *Indian J. Phys., A* **1985**, *59*, 185. (h) CSD refcode APYSAL: Singh, T. P.; Vijayan, M. *Acta Crystallogr., Sect. B: Struct. Commun.* **1974**, *B30*, 557−562.

(5) (a) Bettis, J. W.; Lach, J. L.; Hood, J. *Am. J. Hosp. Pharm.* **1973**, *30*, 240−243. (b) Amos, J. G.; Indelicato, J. M.; Pasini, C. E.; Reutzel, S. M. U.S. Patent 5,412,094, May 2, 1995. (c) *The Merck Index*, 13th ed.; O'Neil, M. J., Ed.; Merck: Whitehouse Station, NJ, 2001; p 325. (d) Bartoszak-Adamska, E.; Wojciechowski, G.; Jaskolski, M.; Brzezinski, B. *J. Mol. Struct.* **2001**, *595*, 21−28. (e) Sangster, J. *J. Phys. Chem. Ref. Data* **1999**, *28*, 889−930.

(6) (a) Walsh, R. D. B.; Bradner, M. W.; Fleischman, S.; Morales, L. A.; Moulton, B.; Rodriguez-Hornedo, N.; Zaworotko, M. J. *Chem. Commun.* **2003**, 186−187. (b) Oswald, I. D. H.; Allan, D. R.; McGregor, P. A.; Motherwell, W. D. S.; Parsons, S.; Pulham, C. R. *Acta Crystallogr., Sect. B* **2002**, *58*, 1057−1066. (c) Bettinetti, G.; Caira, M. R.; Callegari, A.; Merli, M.; Sorrenti, M.; Tadini, C. *J. Pharm. Sci.* **2000**, *89*, 478−489. (d) Oguchi, T.; Tozuka, Y.; Hanawa, T.; Mizutani, M.; Sasaki, N.; Limmatvapirat, S.; Yamamoto, K. *Chem. Pharm. Bull.* **2002**, *50*, 887−891. (e) Remenar, J. F.; Morissette, S. L.; Peterson, M. L.; Moulton, B.; MacPhee, J. M.; Guzman, H. R.; Almarsson, O. *J. Am. Chem. Soc.* **2003**, *125*, 8456−8457. (f) Fleischman, S. G.; Kuduva, S. S.; McMahon, J. A.; Moulton, B.; Walsh, R. D. B.; Rodriguez-Hornedo, N.; Zaworotko, M. J. *Cryst. Growth Des.* **2003**, *3*, 909−919. (g) Oswald, I. D. H.; Motherwell, W. D. S.; Parsons, S.; Pulham, C. R. *Acta Crystallogr., Sect. E: Struct. Rep. Online* **2002**, *58*, 1290−1292.

(7) Stahl, P. H., Wermuth, C. G., Eds. *Handbook of Pharmaceutical Salts: Properties, Selection, and Use*; Wiley: Weinheim, Germany, 2002.

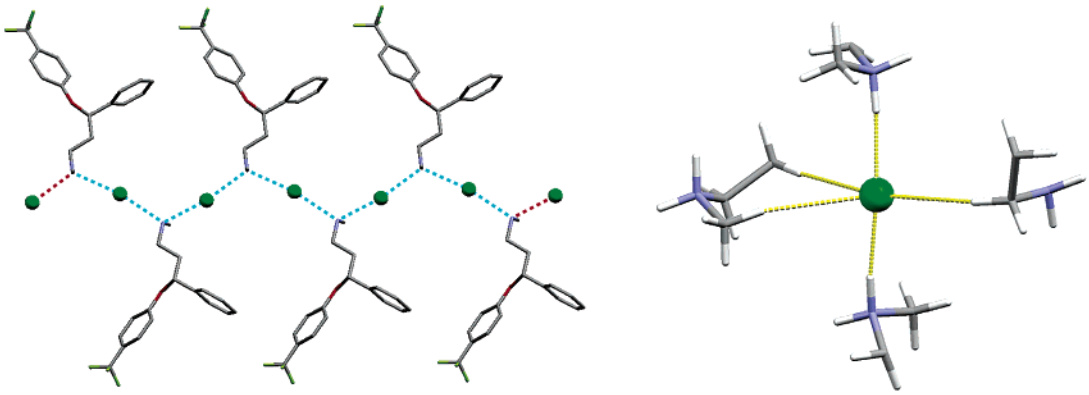

Figure 1. (Left) One-dimensional rod dominant hydrogen bonding motif in the structure of **1**. (Right) Coordination sphere around the chloride ion in **1**, shown with normalized N−H···Cl$^-$ and C−H···Cl$^-$ distances up to 2.8 Å.

series of combinations of ψ and ω scans with 10 s frame exposures and 0.3° frame widths. Data collection, indexing, and initial cell refinements were all carried out using SMART[8] software. Frame integration and final cell refinements were done using SAINT[9] software. The SADABS[10] program was used to carry out absorption corrections.

The structures were solved using direct methods and difference Fourier techniques (SHELXTL version 5.10).[11] Hydrogen atoms were placed at their expected chemical positions using the HFIX command and were included in the final cycles of least squares with isotropic U_{ij}'s related to the atom's ridden upon. The C−H distances were fixed at 0.93 Å (aromatic and amide), 0.98 Å (methine), 0.97 Å (methylene), and 0.96 Å (methyl). All non-hydrogen atoms were refined anisotropically. Scattering factors and anomalous dispersion corrections are taken from ref 12. Structure solution and refinement were performed by using SHELXTL version 5.10 software. Additional details of data collection and structure refinement are given in Table 2.

Dissolution Experiments. Concentrations of fluoxetine hydrochloride in water were determined by UV spectrophotometry at 227 nm. For experiments involving compounds **1**, **3**, and **4**, absorbance values were related to solution concentrations using a calibration curve for **1** ($\epsilon_{227} = 1.23 \times 10^4$ M^{-1}). This was possible since succinic acid and fumaric acid do not absorb at 227 nm and, therefore, did not interfere with determination of the concentration of **1**. Since benzoic acid absorbs at 227 nm, absorbance values for **2** were related to solution concentrations using a calibration curve for **2** ($\epsilon_{227} = 2.06 \times 10^4$ M^{-1}).

For powder dissolution studies of **1**−**4** the starting solids were sieved using ASTM standard mesh sieves to provide samples with approximate particle size ranges of 53−150 μm. In each experiment, a flask containing 30 mL of water was equilibrated at 20.0 °C in a constant-temperature bath. Approximately 800 mg of sample was added to the flask, and the resulting slurry was stirred at 144 rpm using an overhead stirrer equipped with a poly(tetrafluoroethylene) paddle. At each time interval an aliquot of the slurry was withdrawn from the flask and filtered through a 0.2 μm nylon filter. A 0.50 mL portion of the filtered aliquot was diluted to 50.0 mL with water, and a 1.00 mL portion of the diluted solution was then diluted to 10.0 mL with water to provide a total dilution factor of 1000. After the last aliquot was collected, the remaining solids were collected by vacuum filtration, vacuum-dried, and analyzed by XRPD.

Table 1. Hydrogen Bond Distances and Angles to the Chloride Ion in 1[a]

atom–H···atom	atom–H (Å)	H···atom (Å)	atom···atom (Å)	atom–H···atom (deg)
N(1)−H(10)···Cl(1)	1.009	2.092	3.099	175.3
N(1)−H(11)···Cl(1)	1.009	2.117	3.115	169.6
C(2)−H(4)···Cl(1)	1.083	2.693	3.773	175.2
C(10)−H(14)···Cl(1)	1.083	2.756	3.818	166.7
C(1)−H(2)···Cl(1)	1.083	2.769	3.819	163.4

[a] Values are determined using normalized hydrogen distances (N−H = 1.009 Å and C−H = 1.083 Å).

A modified Wood apparatus[17b] was used for intrinsic dissolution experiments. About 200 mg of each sample was compressed into a 0.50 cm^2 disk using a hydraulic press at a nominal gauge pressure of 10 000 psig for 5 min. The disk was compressed to provide a flat surface at one end of the die, and the other end of the die was sealed. A jacketed vessel of about 10 cm internal diameter and 22 cm depth was charged with approximately 1000 mL of an accurately weighed amount of water. The flask was chilled with a circulating bath to provide a water temperature of 10.0 °C, and the assembly containing the compressed sample was placed at the bottom of the vessel with the sample pointing upward. A USP standard paddle was positioned 25 mm above the die, and the solution was stirred at 300 rpm. At each time interval a 6.0 mL aliquot of the solution was withdrawn from the flask and filtered through a 0.2 μm nylon filter. Certain aliquots that were collected toward the end of the run were further diluted with water prior to UV analysis. The linear region of the plot of amount of material dissolved vs time was used to determine the intrinsic dissolution rates, expressed in (mmol of fluoxetine HCl) cm^{-2} min^{-1}.

Results and Discussion

Our strategy is to use the chloride ion as an anchor in the construction of multicomponent amine hydrochloride:guest cocrystals. The exceptional ability of the chloride ion to act as a hydrogen bond acceptor is the key to the approach. In the crystal structure of an amine hydrochloride salt, a charge-assisted hydrogen bond will almost invariably form between the amine cation and the chloride ion. Steiner has noted that "if the cation is capable of donating hydrogen bonds, X−H···Hal$^-$ hydrogen bonds are normally formed and constitute one of the largest contributors to crystal stability."[13] In addition, chloride ions may form hydrogen bonds to weaker, neutral hydrogen bond donors available in the system. These neutral donors play a role in the chloride coordination sphere. For example, when a stronger

(8) SMART, Version 5.624; Bruker AXS, Inc., Analytical X-ray Systems, 5465 East Cheryl Parkway, Madison, WI 53711-5373, 2000.
(9) SAINT, Version 6.02; Bruker AXS, Inc., Analytical X-ray Systems, 5465 East Cheryl Parkway, Madison, WI 53711-5373, 2000.
(10) Sheldrick, G. M. SADABS, Version 2.03; University of Göttingen, Göttingen, Germany, 2001.
(11) SHELXTL, Version 5.10; Bruker AXS, Inc., Analytical X-ray Systems, 5465 East Cheryl Parkway, Madison, WI 53711-5373, 2000.
(12) Wilson, A. J. C., Ed. *International Tables for X-ray Crystallography*; Kluwer Academic: Dordrecht, The Netherlands, 1992; Vol. C, Tables 6.1.1.4 (pp 500−502) and 4.2.6.8 (pp 219−222).
(13) Steiner, T. *Acta Crystallogr., Sect. B* **1998**, *54*, 456−463.

Table 2. Crystallographic Data for Cocrystals 2−4

	2	3	4
empirical formula	$C_{24}H_{25}ClF_3NO_3$	$C_{38}H_{44}Cl_2F_6N_2O_6$	$C_{38}H_{42}Cl_2F_6N_2O_6$
formula wt	467.90	809.06	807.64
temp, K	100(2)	100(2)	100(2)
wavelength, Å	0.710 73	0.710 73	1.541 78
cryst syst	monoclinic	orthorhombic	orthorhombic
space group	$P2_1/n$	*Pbcn*	*Pbcn*
unit cell dimens			
a, Å	14.806(5)	26.620(2)	26.691(8)
b, Å	13.179(4)	7.2147(7)	7.1907(3)
c, Å	24.417(7)	20.8315(19)	20.6546(7)
α, deg	90	90	90
β, deg	97.738(13)	90	90
γ, deg	90	90	90
V, Å^3	4721(2)	4000.8(6)	3958.7(2)
Z	8	4	4
calcd density, Mg/m^3	1.317	1.344	1.355
abs coeff, mm^{-1}	0.210	0.236	2.130
F(000)	1952	1688	1680
cryst size, mm^3	0.47 × 0.15 × 0.10	0.21 × 0.18 × 0.09	0.20 × 0.14 × 0.08
θ range for data collecn, deg	1.52−33.07	1.53−27.50	3.31−58.93
index ranges	$-22 \le h \le 22$, $-20 \le k \le 20$, $-37 \le l \le 37$	$-34 \le h \le 34$, $-9 \le k \le 9$, $-26 \le l \le 27$	$-24 \le h \le 29$, $-7 \le k \le 7$, $-21 \le l \le 22$
no. of rflns collected	82 494	37 123	15 698
no. of indep rflns	17 030 (*R*(int) = 0.0751)	4600 (*R*(int) = 0.0748)	2823 (*R*(int) = 0.1693)
completeness to $\theta = 33.07°$, %	95.0	100.0	99.7
abs cor	semiempirical from equivalents	semiempirical from equivalents	none
refinement method	full-matrix least squares on F^2	full-matrix least squares on F^2	full-matrix least squares on F^2
no. of data/restraints/params	17 030/0/603	4600/0/257	2823/0/257
goodness of fit on F^2	1.052	1.195	1.004
final *R* indices ($I > 2\sigma(I)$)	R1 = 0.0852, wR2 = 0.1930	R1 = 0.0767, wR2 = 0.1855	R1 = 0.0470, wR2 = 0.0927
R indices (all data)	R1 = 0.1330, wR2 = 0.2165	R1 = 0.0892, wR2 = 0.1928	R1 = 0.0941, wR2 = 0.1202
largest diff peak and hole, e Å^{-3}	2.574 and −0.689	0.432 and −0.662	0.561 and −0.747

donor is not available, the ubiquitous C−H donors will often occupy available acceptor sites on the chloride ion.[14] In systems with only a few strong hydrogen bond donors, the hydrogen bond accepting ability of the chloride ion will often be underutilized, and the addition of another strong hydrogen bond donor guest molecule can be accommodated, often by displacing one of the weaker C−H···Cl$^-$ interactions. In comparison to other hydrogen bond acceptors, the chloride ion has several distinct attributes. It is able to accommodate different combinations and numbers of weak and strong hydrogen bond donors, the point location of the negative charge allows it to be placed on symmetry elements such as inversion centers, and its malleable geometric preferences allow it to adopt a variety of hydrogen bonding geometries.

The application of the crystal engineering strategy of combining an amine hydrochloride salt with an additional neutral, strong hydrogen bond donor molecule is demonstrated using fluoxetine hydrochloride as the model API. This approach is expected to be applicable to a variety of pharmaceuticals, because a large percentage of APIs are capable of existing as crystalline hydrochloride salts. For fluoxetine hydrochloride (**1**) only one crystalline phase is known, which is a water- and solvent-free structure.[15] To evaluate the potential for cocrystallization, the structure of **1** was analyzed in terms of the relative strengths of the available hydrogen bond donors and acceptors. The strongest hydrogen bonds in **1**, which are those between the protonated amine donor and the chloride acceptor, form a one-dimensional network (Figure 1). The next strongest donors available are the C−H groups. These form weak hydrogen bonds and complete the nonbonded coordination sphere around the chloride ion (nonbonded distances in Table 1). The chloride ion is an underutilized hydrogen bond acceptor in **1** and may be considered as the focus of attempts to disrupt the homomeric crystal of **1** in favor of a cocrystal by displacing the weak C−H···Cl$^-$ interactions with stronger interactions involving the intended guest molecule.

Of the available pharmaceutically acceptable guest candidates, neutral carboxylic acids stand out as having the best ability to hydrogen bond with chloride ions.[16] We therefore investigated cocrystal formation between fluoxetine hydrochloride and selected pharmaceutically acceptable carboxylic acids. Three cocrystals were isolated. They are cocrystals of **1** with benzoic acid (1:1) (**2**), succinic acid (2:1) (**3**), and fumaric acid (2:1) (**4**). The structure of each cocrystal was determined by single-crystal X-ray diffraction. The relevant crystallographic data are displayed in Table 2. Note that the relative amount of fluoxetine hydrochloride for each cocrystal is high on a weight percent basis: **2**, 74%; **3**, 85%; **4,** 85%. The expected carboxylic acid to chloride hydrogen bond is present in all three structures.

The asymmetric unit of cocrystal **2** is shown in Figure 2. Hydrogen bond parameters are shown in Table 3. The central hydrogen-bonding interactions in **2** result in a zero-dimensional aggregate via the association of two fluoxetine hydrochloride and two benzoic acid molecules (Figure 3). All four of the molecules in the aggregate are crystallographically unique, the independent molecules differing mostly in the region of the $-CF_3$ group on the fluoxetine cation. The aggregate is held

(14) (a) Aakeroy, C. B.; Evans, T. A.; Seddon, K. R.; Palinko, I. *New J. Chem.* **1999**, *23*, 145−152. (b) Aullon, G.; Bellamy, D.; Brammer, L.; Bruton, E. A.; Orpen, A. G. *Chem. Commun.* **1998**, 653−654.

(15) Robertson, D. W.; Jones, N. D.; Swartzendruber, J. K.; Yang, K. S.; Wong, D. T. *J. Med. Chem.* **1988**, *31*, 185−189.

(16) Thallypally, P. K.; Nangia, A. *CrystEngComm* **2001**, 27.

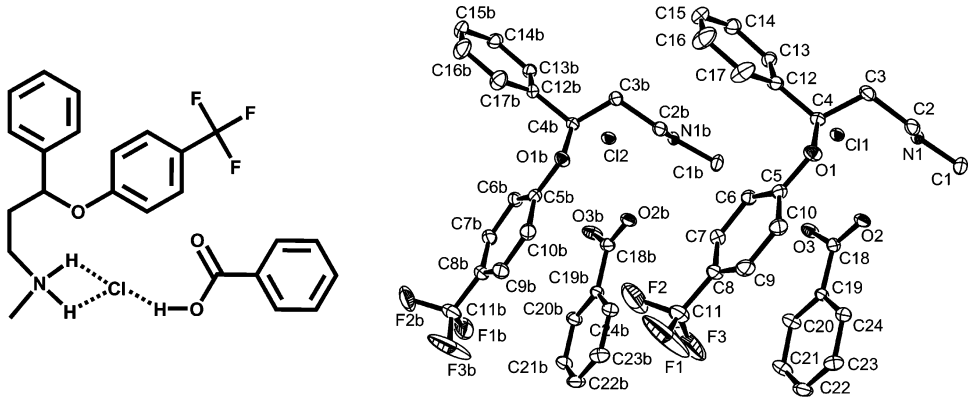

Figure 2. Molecular diagram (left) and ORTEP drawing (right) of the asymmetric unit of **2** (ellipsoids shown at the 50% probability level). Hydrogen atoms have been removed for clarity.

Table 3. Hydrogen Bond Parameters for 2[a]

atom–H···atom	atom–H (Å)	H···atom (Å)	atom··· atom (Å)	atom–H··· atom (deg)
N(1)−H(1D)···O(2)	0.92	2.10	2.789(3)	130.5
N(1)−H(1D)···Cl(1)	0.92	2.56	3.2352(2)	130.3
N(1)−H(1E)···Cl(2)#1	0.92	2.24	3.149(2)	169.2
O(3)−H(3)···Cl(1)	0.84	2.18	3.0197(18)	177.6
N(1B)−H(1B4)···O(2B)	0.92	2.05	2.760(3)	132.8
N(1B)−H(1B4)···Cl(2)	0.92	2.67	3.326(2)	128.7
N(1B)−H(1B5)···Cl(1)#1	0.92	2.22	3.130(2)	168.8
O(3B)−H(3B3)···Cl(2)	0.84	2.19	3.0281(19)	174.7

[a] Symmetry transformations used to generate equivalent atoms: (#1) $-x+1, -y+1, -z$.

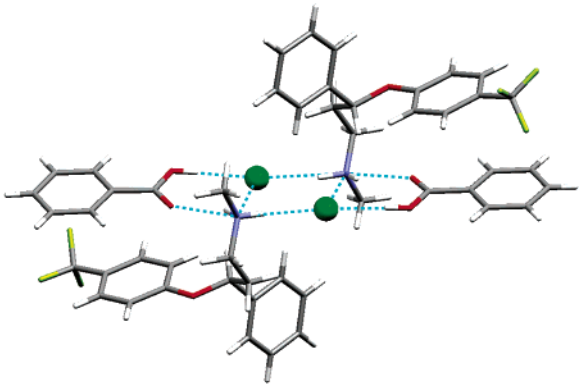

Figure 3. Zero-dimensional aggregate from cocrystal **2**.

together by a cooperative arrangement of N−H···Cl^-, O−H···Cl^-, and N−H···O hydrogen bonds. The aggregates pack (Figure 4) with a combination of van der Waals forces complemented by an aromatic C−H···Cl^- interaction and one activated −CH_3···Cl^- interaction.

The asymmetric units of the isostructural cocrystals **3** and **4**, which consist of one complete fluoxetine hydrochloride molecule and half of one succinic (**3**) or fumaric acid (**4**) molecule, are shown in Figures 5 and 6, respectively. Hydrogen bond parameters are shown in Tables 4 and 5, respectively. The carboxylic acid guest in **3** and **4** is located on an inversion center. The protonated amine forms a bifurcated hydrogen bond to both the carbonyl of the acid group and the chloride ion. The other N−H donor forms a hydrogen bond with the chloride, as does the neutral carboxylic acid. Thus, the chloride accepts three strong hydrogen bonds. There is a two-dimensional layer defined by the carboxylic acid to chloride and protonated amine to

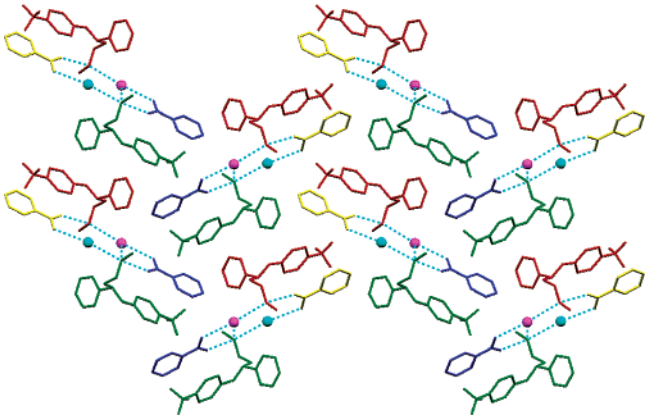

Figure 4. Packing diagram of **2**, with the *bc* plane parallel to the page and symmetry-equivalent molecules shown in solid colors. The fluoxetine cation and the benzoic acid are shown in stick format, and the chloride ions are shown as balls. Hydrogen bonds are shown in blue.

chloride hydrogen bonds (Figure 7). These layers are stacked as shown in Figure 8.

Each cocrystal was characterized using X-ray powder diffraction (XRPD), differential scanning calorimetry (DSC), thermogravimetric analysis (TGA), Raman spectroscopy, and automated moisture sorption/desorption analysis. These data are available in the Supporting Information. The XRPD patterns obtained for each cocrystal were compared to the pattern of the fluoxetine HCl starting material in order to confirm that new solid phases were formed (Figure 9). The Raman spectra also indicated new solid phases. Moisture sorption/desorption experiments showed that each cocrystal is nonhygroscopic, undergoing less than 0.2% weight gain up to 95% relative humidity.

The melt endotherms obtained from the DSC data are shown in Table 6 along with the literature melting points for the corresponding cocrystal components. The melting points of cocrystals **2** and **4** are between the melting points of the pure starting materials (**1** and the acid guest), while the melting point of **3** is lower than that of either component. Although cocrystals **3** and **4** are isostructural, the melting points are quite different. The melting point of **3** is lower than that of either succinic acid or fluoxetine hydrochloride, while the melting point of **4** is higher than that of fumaric acid. The melting points of these two isostructural cocrystals highlight the difficulty in correlating the effect of structural variation with the resulting change in physical properties.

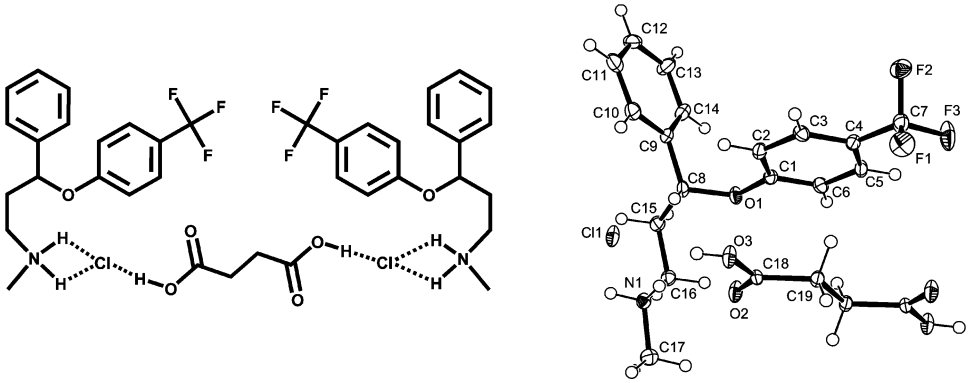

Figure 5. Molecular diagram (left) and ORTEP drawing (right) of the asymmetric unit of **3** (ellipsoids shown at the 50% probability level).

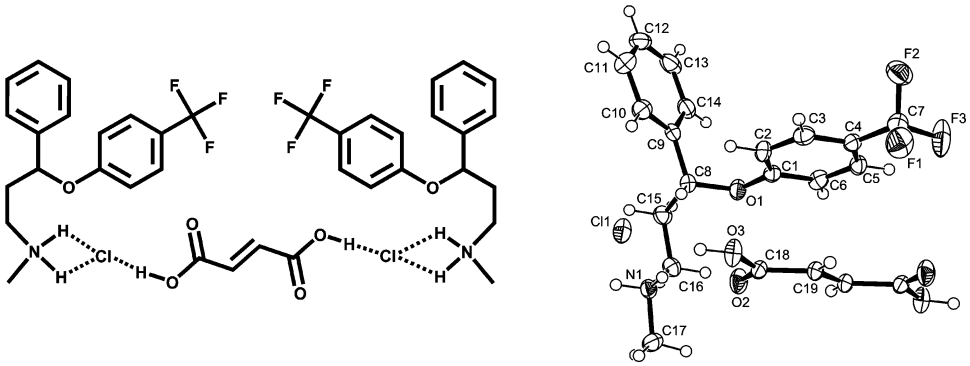

Figure 6. Molecular diagram (left) and ORTEP drawing (right) of the asymmetric unit of **4** (ellipsoids at the 50% probability level).

Table 4. Hydrogen Bond Parameters for 3[a]

atom-H···atom	atom–H (Å)	H···atom (Å)	atom··· atom (Å)	atom-H··· atom (deg)
O(3)−H(3A)···Cl(1)	0.82(4)	2.21(4)	3.028(2)	173(4)
N(1)−H(1A)···O(2)	0.85(4)	2.22(4)	2.842(3)	130(4)
N(1)−H(1B)···Cl(1)#2	0.89(5)	2.26(5)	3.128(3)	164(4)
N(1)−H(1A)···Cl(1)	0.85(4)	2.61(4)	3.258(3)	135(3)

[a] Symmetry transformations used to generate equivalent atoms: (#1) $-x, -y + 1, -z$; (#2) $-x + {}^1/_2, y - {}^1/_2, z$.

Table 5. Hydrogen Bond Parameters for 4[a]

atom–H···atom	atom–H (Å)	H···atom (Å)	atom··· atom (Å)	atom–H···atom (deg)
N(1)−H(1A)...Cl(1)	0.92(4)	2.55(4)	3.230(3)	131(3)
N(1)−H(1A)...O(2)	0.92(4)	2.19(4)	2.871(4)	131(3)
N(1)−H(1B)...Cl(1)#2	0.91(3)	2.24(3)	3.136(3)	169(3)
O(3)−H(3A)...Cl(1)	0.88(3)	2.14(3)	3.015(2)	173(3)

[a] Symmetry transformations used to generate equivalent atoms: (#1) $-x + 2, -y + 2, -z + 2$; (#2) $-x + {}^3/_2, y - {}^1/_2, z$.

Powder dissolution profile experiments were carried out on compounds **1**−**4** at 20 °C. All compounds dissolve at a rapid rate such that differences in the powder dissolution rates could not be discerned at the early time points. These results are presented in graphical form in Figure 10. The data for the cocrystals is normalized such that the solution concentration of fluoxetine hydrochloride (mM) is plotted for each compound. This type of analysis permits a direct comparison of the effect of the acid guest molecule in the cocrystal on the solubility of the API. The solubility values for the cocrystals expressed in mg/mL of the fluoxetine component as well as the cocrystal are provided in Table 7. Since solubility and bioavailability are often related, these results demonstrate that, in principle, cocrystals can be used to tune the bioavailability of an API.

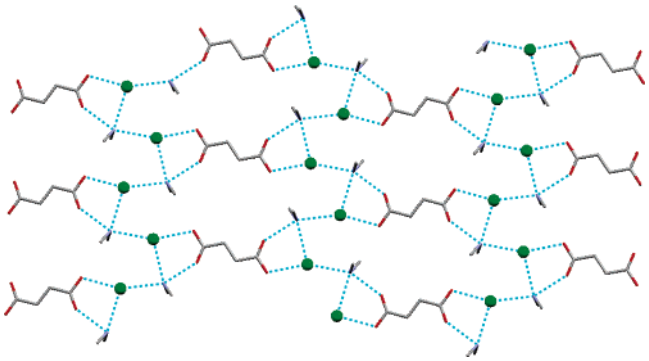

Figure 7. Layered structure in cocrystal **3**. The fluoxetine atoms have been removed, except for the cationic C−NH_2^+−C moiety, for clarity. Intra-ion bonding forms a one-dimensional, charge-assisted motif along the *b* axis (vertical), which is bridged by neutral succinic acid interactions along the *a* axis (horizontal). An identical motif exists in **4**.

Fluoxetine hydrochloride and cocrystals **2** and **4** were stable in water at 20 °C such that the equilibrium solubility values could be obtained at this temperature (Table 7). The stability of **1**, **2**, and **4** was demonstrated by isolating the undissolved solids after several hours and then analyzing the solids by XRPD. In these three experiments, the corresponding XRPD patterns matched those obtained for the starting solid phases. For cocrystal **3**, XRPD analysis of the solids isolated after several hours provided a pattern corresponding to fluoxetine hydrochloride, which demonstrates that **3** dissociated and recrystallized to fluoxetine hydrochloride under the conditions of the powder dissolution experiment. The succinic acid component of this cocrystal remains in solution due to its high solubility, and consequently succinic acid is not observed in

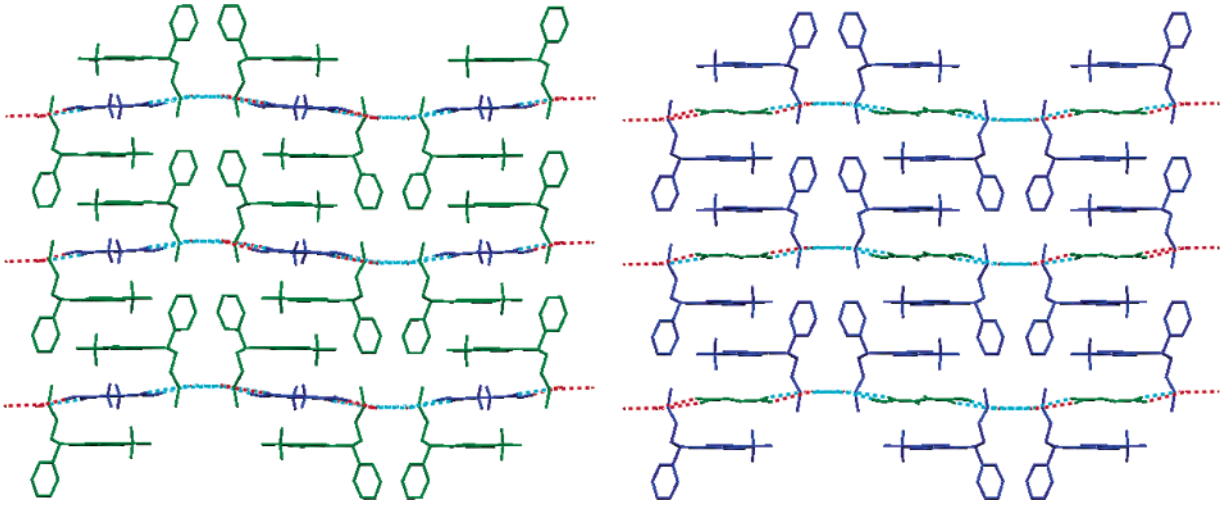

Figure 8. Isostructural cocrystals of fluoxetine hydrochloride with succinic acid (**3**, left) and fumaric acid (**4**, right). View is of the *ac*-plane. Hydrogen atoms on the fluoxetine cation have been removed, and entire molecules appear in a single color for clarity.

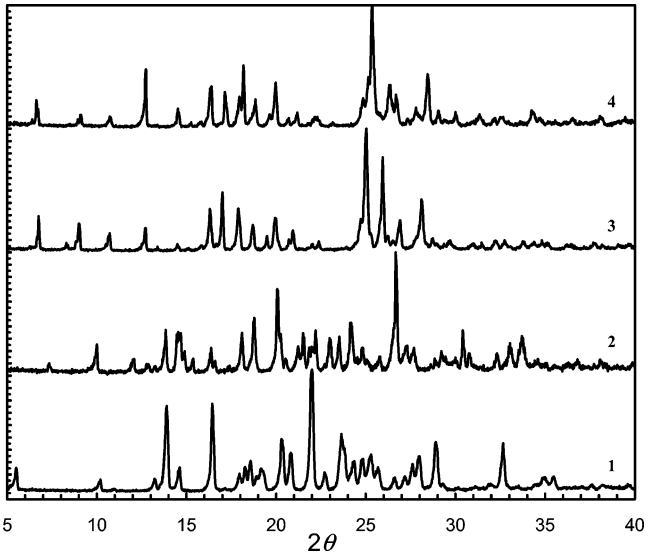

Figure 9. Comparison of the experimental XRPD patterns for **1**−**4**.

Table 6. Melting Point and DSC Data for Cocrystals 2−4 and the Related Individual Components

compd	endotherm onset (°C)	heat of fusion (J/g)	lit. mp[a] (°C)
fluoxetine HCl (**1**)	157.2	105	158.4−158.9
fluoxetine HCl:benzoic acid (1:1) (**2**)	131.5	119	
benzoic acid			122.4
fluoxetine HCl:succinic acid (2:1) (**3**)	134.1	109	
succinic acid			185−187
fluoxetine HCl:fumaric acid (2:1) (**4**)	161.1	108	
fumaric acid			∼287

[a] Values obtained from ref 12.

the XRPD pattern of the recovered solids after the powder dissolution experiment. The instability of **3** in water is also characterized by the powder dissolution profile of this cocrystal (Figure 10). Unlike the other systems studied, the rapid increase in fluoxetine hydrochloride concentration at the early time points is followed by a decrease in concentration, which is a result of the recrystallization of the cocrystal to fluoxetine hydrochloride. The peak fluoxetine hydrochloride concentration for **3** is roughly double that for API alone, while the equilibrium concentration

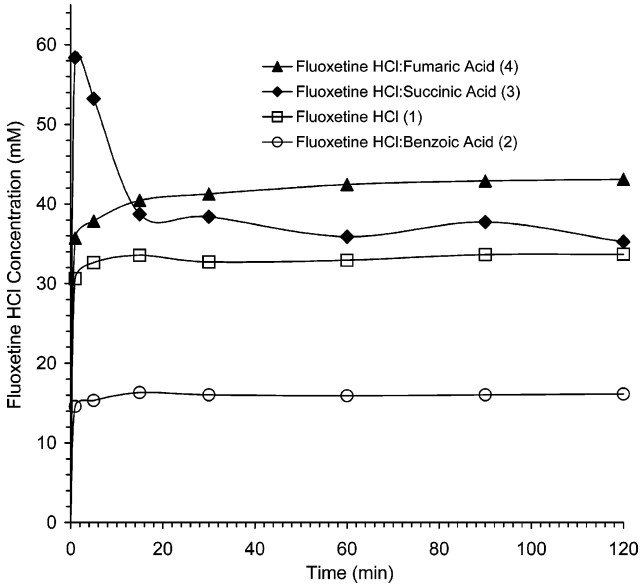

Figure 10. Powder dissolution profiles for **1** (□), **2** (○), **3** (◆), and **4** (▲) in water at 20 °C.

of the API in **4** is approximately 30% higher than **1** alone (Table 7). The increase in solubility of **3** and **4** relative to **1** demonstrates the potential for cocrystal engineering to increase the bioavailability of an API.

Intrinsic dissolution rate experiments[17] were performed in order to obtain quantitative information on the dissolution rates of compounds **1**−**4**, which were not apparent from the powder dissolution experiments described above. The intrinsic dissolution studies were carried out in water at 10 °C in order to decrease further the dissolution rates such that they could be measured reliably. These results are graphed in Figure 11. The data have been normalized to represent the rate of dissolution of the fluoxetine hydrochloride component for each of the cocrystals so that an evaluation of the dissolution of the API could be directly compared. Only the linear region of the dissolution profile is shown in Figure 11, which roughly

(17) (a) Milosovich, G. J. *J. Pharm. Sci.* **1964**, *53*, 484−487. (b) Wood, J. H.; Syarto, J. E.; Letterman, H. *J. Pharm. Sci.* **1964**, *53*, 1068−1077. (c) Grant, D. J. W.; Higuchi, T. *Solubility Behavior of Organic Compounds*; Techniques of Chemistry Series 21; Wiley: New York, 1990; Chapter XI.

Table 7. Aqueous Solubility and Intrinsic Dissolution Rates for 1−4 at 20 °C

	equilibrium solubility at 20 °C			intrinsic dissolution rate at 10 °C	
compd	[fluoxetine HCl] (mM)	[fluoxetine HCl] (mg/mL)	[cocrystal] (mg/mL)	fluoxetine HCl (mmol cm^{-2} min^{-1})	k_{rel} ($k(n)/k(1)$)
fluoxetine HCl (**1**)	33.1	11.4	n/a	6.8×10^{-3}	1
fluoxetine HCl:benzoic acid (1:1) (**2**)	16.1	5.6	7.5	3.4×10^{-3}	0.5
fluoxetine HCl:succinic acid (2:1) (**3**)	58.4[a]	20.2[a]	23.6[a]	$>1.9 \times 10^{-2}$ [b]	>2.9[b]
fluoxetine HCl:fumaric acid (2:1) (**4**)	42.9	14.8	17.3	6.1×10^{-3}	0.9

[a] Maximum concentration measured at 1 min. [b] Intrinsic dissolution rate of **3** was too rapid to provide an accurate value.

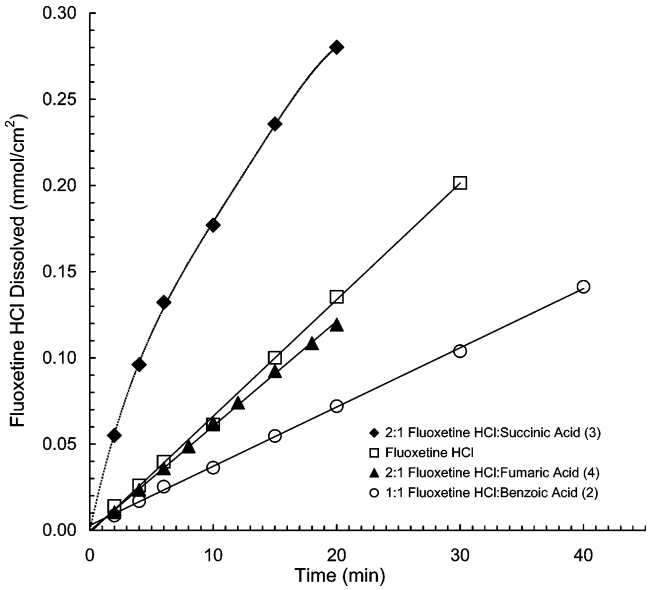

Figure 11. Intrinsic dissolution profiles for **1** (□), **2** (○), **3** (◆), and **4** (▲) in water at 10 °C.

corresponds to 10% dissolution of the total charge of starting material. The dissolution of **3** was too fast to measure an accurate value for the intrinsic dissolution rate at this temperature. The values for **1**, **2**, and **4** obtained by least-squares analysis of the linear regions are provided in Table 7. For **3** an approximate 3-fold increase in the dissolution of the API relative to **1** can be estimated from the early points in the experiment. In contrast, cocrystal **2** dissolves at a rate that is approximately half of the rate for the API alone, while the dissolution rate for **4** is roughly similar to that for **1**. These results demonstrate that, by cocrystallizing an API with different guest molecules, it is possible to increase or decrease the dissolution rate of the API or to leave the effective dissolution rate essentially unchanged.

The manner in which the structural and thermodynamic factors influence the corresponding dissolution rate is presently unknown for these compounds. Regardless of these factors, it is interesting to note that the aqueous solubility of the guest molecule appears to correlate to the aqueous dissolution rates of the corresponding cocrystal with fluoxetine hydrochloride. Approximate solubilities in water are as follows: benzoic acid, 0.34 g/100 g at 25 °C;[18] succinic acid, 7.5 g/100 g at 25 °C;[19] fumaric acid, 0.61 g/100 g at 25 °C.[20] These follow the same ordering as the values for the intrinsic dissolution rate (Table 7).

Conclusions

The ability to alter the physical properties of a crystalline solid containing an API by incorporating a pharmaceutically acceptable molecular species into a unique crystal lattice presents an opportunity to tailor the properties of a solid-state dosage form at the molecular level. By using crystal engineering strategies[21] to guide the selection of API:guest combinations that are preorganized to form complementary intermolecular hydrogen bonds, the potential for discovering useful cocrystals is increased and the number of API:guest combinations that must be empirically examined is reduced.

The viability of a crystal engineering approach to the identification of stable cocrystals has been demonstrated through the rational synthesis of cocrystals of fluoxetine hydrochloride with fumaric, succinic, and benzoic acids. In all three cases the organic acid was found to engage in a hydrogen bond with the targeted chloride ion. These three cocrystals were prepared in gram quantities using standard techniques. The solubility and intrinsic dissolution rate experiments conducted on fluoxetine hydrochloride and the corresponding cocrystals demonstrated that these species have significantly different solubilities and dissolution rates. These results indicate that it is possible to alter the physical properties of the solid-state form of an API through the application of API:guest cocrystals.

We have tested this crystal engineering approach with five other amine hydrochloride APIs in order to determine if the neutral carboxylic acid guest to chloride acceptor synthon is a robust and reliable design tool. Cocrystals with neutral carboxylic acids have been observed in all cases, and the expected neutral organic acid to chloride hydrogen bond is present in all of the structures. These results will be the subject of future contributions.

Acknowledgment. We thank Dr. Kenneth Hardcastle and Dr. Karl Hagen from the Emory University X-ray Diffraction Center for determining the crystal structures reported in this paper.

Supporting Information Available: X-ray crystallographic information files (CIF) for cocrystals **2**−**4** and figures giving Raman, XRPD, TGA, DSC, and moisture sorption/desorption data for compounds **1**−**4**. This information is available free of charge via the Internet at http://pubs.acs.org.

JA048114O

(18) *The Merck Index*, 13th ed.; Merck & Co.: Whitehouse Station, NJ, 2001 (CD-ROM).
(19) Wermuth, C. G.; Stahl, P. H. In *Handbook of Pharmaceutical Salts: Properties, Selection, and Use*; Stahl, P. H., Wermuth, C. G., Eds.; Verlag Helvitica Chimica Acta: Zurich and Wiley-VCH: Weinheim, Germany, 2002; p 306.
(20) Reference 13, p 282.
(21) (a) Aakeroy, C. B. *Acta Crystallogr., Sect. B: Struct. Commun.* **1997**, *53*, 569−586. (b) Bilton, C.; Allen, F. H.; Shields, G. P.; Howard, J. A. K. *Acta Crystallogr. Sect. B: Struct. Commun.* **2000**, *56*, 849−856. (c) Coe, S.; Kane, J. J.; Nguyen, T. L.; Toledo, L. M.; Wininger, E.; Fowler, F. W.; Lauher, J. W. *J. Am. Chem. Soc.* **1997**, *119*, 86−93. (d) Desiraju, G. R. *Angew. Chem., Int. Ed. Engl.* **1995**, *34*, 2311−2327. (e) Desiraju, G. R. *Chem. Commun.* **1997**, 1475−1482. (f) Nangia, A.; Desiraju, G. R. *Acta Crystallogr., Sect. A* **1998**, *54*, 934−944. (g) Videnova-Adrabinska, V. *Acta Crystallogr., Sect. B* **1996**, *B52*, 1048−1056.